International Journal of Emerging Engineering and Technology (IJEET)
ISSN (e): 2958-3764
Volume: 4, Number: 2, Pages: 15 - 19, Year: 2025

Electro-Mechanical Characteristic Analysis of the Surface Mounted Permanent Motor

Qurban Ali Shah Syed[1,*], Kamran Ahmed Samo[2] and Zahid Muhammad[3]

[1,2] Department of Electrical Engineering, The University of Larkano, Larkana, 77150, Pakistan
[3] Department of Electrical Engineering, Isra University, Hyderabad, 71000, Pakistan
[*] Corresponding author: Qurban Ali Shah Syed (Email: qurban.syed@uolrk.edu.pk)

Received: 21/06/2025, Revised: 15/10/2025, Accepted: 17/12/2025

***Abstract*—This paper presents a detailed electro-mechanical performance analysis of the three-phase brushless DC (BLDC) surface-mounted permanent magnet (SPM) motor. The BLDC SPM motor operates at the rated load and rated constant rated speed conditions. The electro-mechanical characteristics of the BLDC SPM motor include the air-gap magnetic flux distribution, mechanical torque, torque ripple, mechanical output power and electro-mechanical losses. The two-dimensional (2D) finite element analysis (FEA) is utilized to model and numerical analysis of the BLDC SPM motor.**

***Index Terms*—BLDC motor, electrical machines, electro-mechanical conversion, finite element analysis, permanent magnet (PM), SPM motor.**

I. INTRODUCTION

RECENTLY, the permanent magnet synchronous motors (PMSMs) are becoming a dominant solution to the modern electric drive applications [1], because of their high efficiency and power density, and excellent dynamic performances [2]. Among different PMSM configurations, the surface-mounted permanent magnet (SPM) motors have gained significant attention in applications, such as electric vehicles (EVs), aerospace actuators, industrial automation, and renewable energy systems [1]-[2]. The popularity of the SPM motors is attributed to their simple rotor structure, reduced manufacturing complexity, and reliable electromagnetic behaviour [3].

In an SPM motor, the permanent magnets (PMs) are mounted directly on the rotor surface, resulting in a nearly uniform air-gap magnetic field [4]. The SPM structure leads to a predominantly sinusoidal back electromotive force (EMF) and minimizes the magnetic saliency [4]. Therefore, the SPM motors have almost equal direct and quadrature (d and q) axis inductances. Hence, the control strategies are simpler, and field-oriented control (FOC) proved suitable across a wide range of operating conditions for the SPM motor [5].

At rated load operation, the electromagnetic behavior of the SPM motor is governed by the combined magnetic field of the PM excitation and the stator current excitation effects [4]. Unlike the no-load conditions presented in [6], the interaction between the armature reaction and the magnet field significantly influences the air-gap flux distribution, electromagnetic torque production, and losses [5]-[6]. Accurate analysis of the rated-load electromagnetic characteristics is indispensable for the realistic performance assessment and robust motor design [7].

Compared to the interior permanent magnet (IPM) motor, the defining features of the SPM motor is its negligible magnetic saliency because the PMs are mounted on the rotor surface without flux-barrier structures [8]. Therefore, almost equal d- and q-axis inductances lead to torque production predominantly from electromagnetic rather than reluctance-based sources [5]. Under rated-load conditions, the electromagnetic torque is mainly proportional to the q-axis current; therefore, simplified control strategies are adopted, and the electromagnetic field distribution in the torque optimisation is emphasised [5].

The air-gap magnetic flux density under rated load conditions deviates from its no-load conditions due to the armature reaction produced by the stator currents [7]. This reaction can cause the magnetic saturation in the stator teeth and yoke, altering the effective flux linkage and impacting the electromagnetic torque linearity [8]. Thus, nonlinear electromagnetic effects need to be evaluated to ensure accurate prediction of SPM motor performance [9].

The electromagnetic torque characteristics at rated load are the key performance indicators for the SPM motors. The torque ripples are generated due to the interaction of the harmonic components in the air-gap magnetic field, winding distribution, and inverter-supplied currents. The torque ripples lead to vibration, acoustic noise, and reduced mechanical lifespan [10]. Therefore, improving the electromagnetic torque and reducing torque ripple under rated load conditions are essential for improving the motor drive smoothness and system reliability [11].

The copper and iron losses are significantly influenced by the electromagnetic conditions at the rated load [12]. At the rated

current, the copper losses dominate due to the increased stator current density, while the iron losses are affected by the magnetic flux density levels and harmonic content in the magnetic core [11]-[12]. Both losses directly impact the SPM motor efficiency, thermal behaviour, and continuous operation capability. Therefore, accurate electromagnetic evaluation is an important aspect of the motor's rated-load analysis [12].

The back EMF under stator's current excitation is different from the no-load back-EMF due to the magnetic saturation and cross-coupling effects [10]-[12]. The variation in the back-EMF influences the voltage utilization, the field-weakening capability, and inverter sizing. Thus, the understanding of the electromagnetic interactions of the SPM motor is important for ensuring its stable operation at rated speed and torque [9], [11].

Analytical methods, numerical method such as finite element analysis (FEA), and / or the experimental measurements are commonly employed to evaluate the electro-mechanical characteristics of the SPM motors [13]. While analytical models offer physical insight and rapid evaluation, the FEA numerical method enables the detailed investigation, especially when there are the complex geometries, nonlinear magnetic behavior, and slotting effects of the SPM machines [13]-[14]. Experimental validation remains indispensable for verifying the accuracy of theoretical and numerical predictions [13].

This paper presents a detailed and comprehensive analysis of the electro-mechanical behavior of the brushless DC (BLDC) SPM motor operating at rated load. Thus, the air-gap magnetic flux distribution, the mechanical torque production, electro-mechanical loss mechanisms, and saturation effects are discussed and computed using the 2D FEA tutored by [14-16].

II. BLDC SPM Motor

The BLDC motor is characterized by the specific geometric and physical dimensions, designed for the pump applications. The BLDC SPM motor assembly comprises a fixed part stator and a movable part rotor, separated by an air gap, as shown in Fig. 1. The stator includes yoke, slots, and three-phase windings, while the rotor iron holds the surface-mounted PMs.

Key physical characteristics of the BLDC SPM motor include 24 stator slots, a 3-phase Y-connection, and 2 pole pairs, as shown in Fig. 1. The three-phase BLDC SPM motor utilizes the NdFeB magnets mounted on the rotor. Whereas, the stator of the BLDC SPM motor's winding is 3-phase with a classical concentric type having a throw of 5 coils, and 1 coil per pole per phase, as shown in Fig. 2.

The three-phase BLDC SPM motor's outer diameter is 48 mm, and its stack length is 50.308 mm. The airgap length is 0.503 mm. The rotor's shaft radius is 9.003 mm, and the rotor's external radius is 25.154 mm. The PMs are mounted on the rotor and has a thickness of 6.987 mm with a PM pole arc of 150°. The stator slots are square-shaped with a radial depth of 14 mm, slot opening of 1.5 mm and the tooth width of 3.4 mm.

III. Methodology

The 2D FEA simulation method for the BLDC SPM motor performance at constant speed, specifically focusing on the electromagnetic torque is addressed [14]. The 2D FEA simulates the BLDC SPM motor operating at a constant speed of 1000 rpm, driven by a 3-phase bridge electric circuit. Thus, the BLDC SPM motor performances are computed, including shaft torque and electrical power consumption, while considering factors like airgap magnetic field, spectrum analysis, core and magnet losses, and current components.

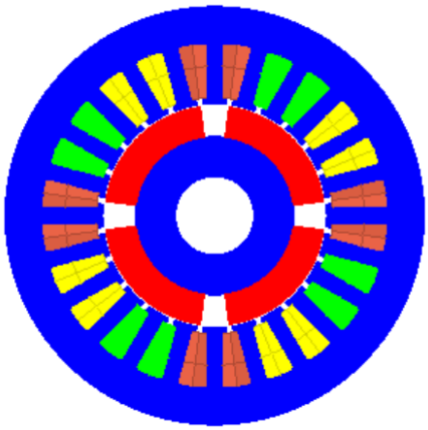

Fig. 1. Three-phase BLDC SPM motor.

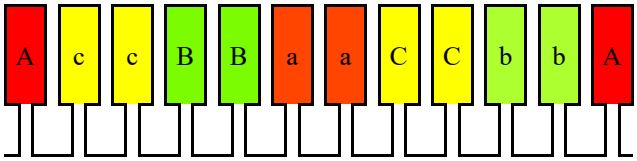

Fig. 2. Three-phase base-winding scheme for the BLDC SPM motor.

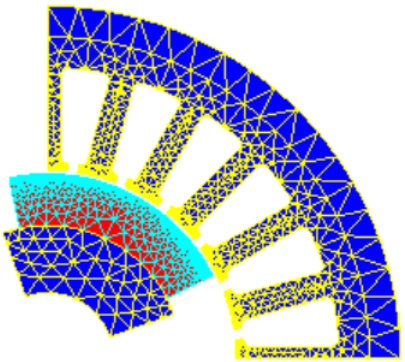

Fig. 3. Meshing of the BLDC SPM motor.

Geometry: The geometry step defines the physical shape of the BLDC SPM motor being simulated, as shown in Fig. 1. The main parts of the BLDC SPM motor, such as, the stator, rotor, PMs, air gap, shaft, and surrounding air region are created with their actual dimensions. Symmetry and periodicity are utilized to reduce the geometrical size and computation time.

Meshing: Meshing discretized the geometry and divides the geometry into a large number of small elements, as shown in Fig. 3 to compute the electro-mechanical quantities, using the

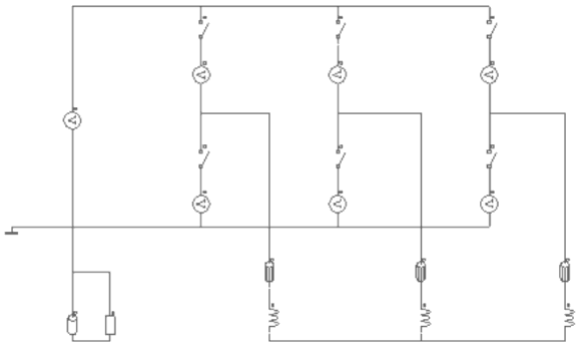

Fig. 4: Stator current excitation circuit for the three-phase quasi square current.

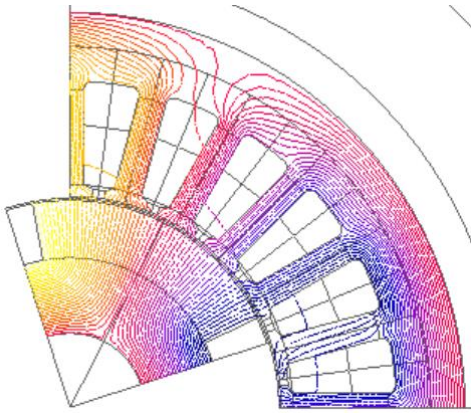

Fig. 5: Magnetic flux lines when the rotor is at 0.003 sec.

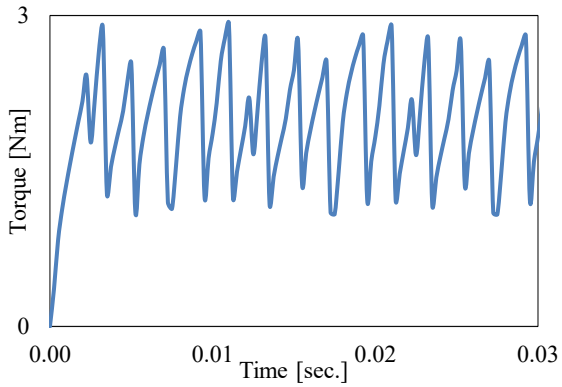

Fig. 6. Electromagnetic torque of the three-phase BLDC SPM motor.

FEA. Line meshing is adopted, and finer mesh regions are applied where the field changes rapidly, such as in the air gap, PMs, and stator teeth as shown in Fig. 3. However, coarser meshes are used elsewhere to reduce the FEA computation time. The better meshing ensures the numerical accuracy and stability of the solution.

Physical application: For the FEA for the electromagnetic analysis of the BLDC SPM motor at rated load conditions and constant speed, a 2D transient magnetic application is selected. Hence, the magnetic field is solved as a function of time. The respective materials are selected and assigned to different regions, such as electrical steel for the stator and rotor core, the PM material for the magnets and air for the air gaps and surroundings. Mechanical sets are defined to differentiate the fixed parts, such as, stator, its windings and stationary airgap from the moving parts such as, rotor, its PMs and rotatory airgap. The electrical circuits are also created to represent the windings, power supply, and switching elements, as shown in Fig. 4.

Physics: The BLDC SPM motor operates at constant speed under electrical excitation. The rotor speed of the BLDC SPM motor is imposed and kept constant at 1000 rpm. However, the stator is fixed and is driven by the three-phase inverter supplying quasi-square-wave currents, as shown in Fig. 4. The electrical circuit of the BLDC SPM motor is modified to include switches, voltage sources, and control logic based on the rotor position. Eddy current effects in the PMs and losses in the iron are enabled by assigning the appropriate material properties, such as, magnetization characteristics and directions. Thus, the realistic interaction between the electromagnetic fields, motion, and electrical supply is properly assigned and guided [17-19].

Solving: The time-controlled simulation scenario of the BLDC SPM motor is created, and the solver advances step by step in time, updating the rotor position, magnetic field distribution, currents, and voltages at each time step. The time step is chosen carefully to capture both the electrical switching and the mechanical motion accurately. The solver iterates until convergence is reached at every step, producing a complete transient solution over one or more electrical periods.

Post-processing: The results are post processed to analyze and interpret the simulation results. The magnetic flux density plots are examined to verify the magnetic field distribution and saturation levels. The magnetic flux flow path is shown in Fig. 5. The mechanical torque and mechanical power are calculated from the electromagnetic forces. The electrical quantities such as the phase currents and Joule losses are evaluated. Thus, the raw simulation data is transformed into a meaningful performance indicator of the three-phase BLDC SPM motor.

IV. Results and Discussions

A. Mechanical performance

The mechanical torque output waveform of Fig. 6 illustrates the torque generated by the BLDC SPM motor over time. The mechanical torque waveform provides the insights into the dynamic performance of the three phase DLDC SPM motor under rated load operating conditions. The average mechanical torque of the BLDC SPM motor is 1.979 Nm.

The mechanical torque waveform shows a fluctuating pattern, indicating the torque ripple of 1.727 Nm. The torque ripple needs to be reduced as it is unwanted for the smooth operation of the BLDC SPM motor. The torque ripples in the BLDC SPM motor are generated due to the various factors, including the motor's design, the interaction between the PMs and stator slots, and the motor control strategy. Thus, analyzing the electro-mechanical characteristic of the three-phase DLDC SPM motor is important for understanding the motor's

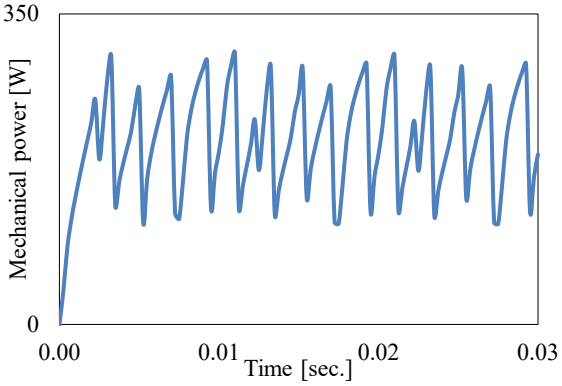

Fig. 7. Mechanical output power of the BLDC SPM motor.

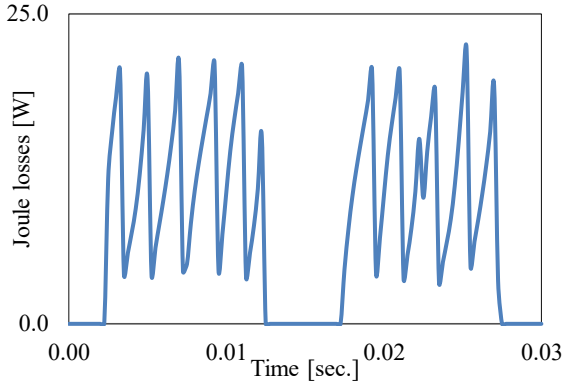

Fig. 8. Joule losses waveform.

smoothness of operation and the potential vibrations.

From the mechanical torque τ, the output mechanical power P is computed using the $P = \tau\omega$ relation, where angular velocity is ω. The average output mechanical power is 206 W, as shown in Fig. 7. The output mechanical power is calculated from the relation of the mechanical torque and angular speed. Mechanical power is important for evaluating the BLDC SPM motor's overall power delivery capability.

Understanding the mechanical torque waveform is important for the electrical motor designers to optimize the motor performance, minimize undesirable torque ripples, and ensure the efficient electro-mechanical power conversion. When the three phase BLDC SPM motor operates at a constant speed of 1000 rpm, the motor exhibits various types of losses that contribute to the reduction of overall efficiency. These losses include the Joule losses, mechanical losses, core losses, and magnet losses. Thus, the overall efficiency of the motor is calculated based on these losses and the output mechanical power.

B. Electro-Mechanical Losses

Joule losses commonly known as the copper losses or I^2R losses occur primarily due to the resistance of the stator windings. Thus, the Joule losses are calculated from the root mean square (rms) value of the current I passing through the coil conductors. Thus, the rms current of 10.33 A, leads the Joule losses of 22.77 W for the three phases, as shown in Fig. 8. Similarly, the mechanical losses of the three-phase BLDC SPM motor are determined to be 7.5 W.

C. Electrical performance

The current waveform of the BLDC SPM motor is shown in Fig. 9, and it is determined by removing the current component from the Joule losses of Fig. 8. The calculated rms output current of the BLDC SPM motor is 10.12 A. Similarly, the voltage induced during the interaction of the magnetic and electric excitation of the three-phase BLDC SPM motor is shown in Fig. 10. The calculated rms voltage of the three-phase BLDC SPM motor is 9.166 V.

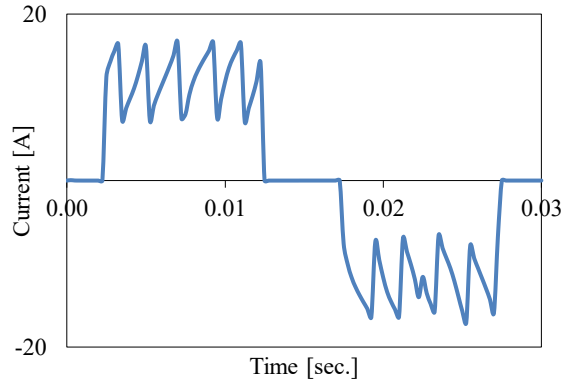

Fig. 9. Joule losses waveform.

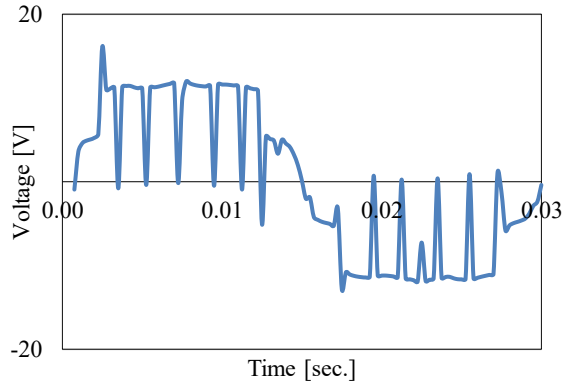

Fig. 10. Voltage when the three-phase BLDC SPM motor's stator is excited.

V. Conclusion

The three-phase BLDC SPM motor for pump application is investigated and numerically simulated using the 2D FEA. The BLDC SPM motor runs at the rate load with constant speed and its stator is excited along with the rotor. Thus, the electro-mechanical characteristics of the three phase BLDC SPM motor are analyzed due to the interaction of the current and magnetic excitation.

At constant speed, the BLDC SPM motor provides critical insights into its electromagnetic torque characteristics, thus, the mechanical characteristics are analyzed. The mechanical torque characteristics reveals torque ripple, which is a common phenomenon in the BLDC SPM motors, and it is influenced by

the design and its control strategies. The reduction of the torque ripples enhances the mechanical torque, and it is aimed for the future investigation. Reducing the torque ripple is essential for ensuring the smooth operation and reduction in vibration of the BLDC SPM motor.

The mechanical torque quantifies the output mechanical power, and the yielded average mechanical power is 206 W. The mechanical output power is crucial for assessing the BLDC SPM motor's overall power delivery capabilities under its specific operating conditions.

The electrical performance of the three-phase BLDC SPM motor is quantified by measuring current, voltage, and electrical losses. The total Joule losses are 22.7 W, and mechanical losses are 7.5 W; thus, the efficiency of the BLDC SPM motor reduces when both electromechanical losses and core and magnetic losses are accumulated..

The future work is aimed at reducing the torque ripples and control strategies to ensure the motor's smooth operation. The core losses and magnetic losses need to be numerically determined. Thus, a comprehensive future study is aimed at the electromagnetic performance of the three-phase BLDC SPM motor at no load, rated load and over and under load operation conditions for the pump application.

ACKNOWLEDGEMENT

Corresponding author acknowledges the support of Altair® for the FEM license during the PhD research at the chair of Electrical Drives and Machines, FAU University of Erlangen-Nuremberg. The simulation and technical process is adopted from the Flux solver manual.

CONFLICTS OF INTEREST

The authors declare no conflicts of interest to report regarding the present study.

AUTHOR CONTRIBUTIONS

Conceptualization, methodology, software, validation, writing—original draft preparation, Q. A. S. Syed; writing—review and editing, Q. A. S. Syed, K. A. Samo and Z. Muhmmad.

FUNDING STATEMENT

This research received no external funding.

INSTITUTIONAL REVIEW BOARD STATEMENT

Not applicable.

INFORMED CONSENT STATEMENT

Not applicable.

DATA AVAILABILITY STATEMENT

Data is available on reasonable request.

REFERENCES

[1] Nategh, Shafigh, Aldo Boglietti, Yujing Liu, Daniel Barber, Ron Brammer, David Lindberg, and Ola Aglen. "A review on different aspects of traction motor design for railway applications." *IEEE Transactions on Industry Applications* 56, no. 3 (2020): 2148-2157.

[2] De Santiago, Juan, Hans Bernhoff, Boel Ekergård, Sandra Eriksson, Senad Ferhatovic, Rafael Waters, and Mats Leijon. "Electrical motor drivelines in commercial all-electric vehicles: A review." *IEEE Transactions on vehicular technology* 61, no. 2 (2011): 475-484.

[3] C. Liu, K. T. Chau, C. H. T. Lee and Z. Song, "A Critical Review of Advanced Electric Machines and Control Strategies for Electric Vehicles," in *Proceedings of the IEEE*, vol. 109, no. 6, pp. 1004-1028, June 2021.

[4] S. Q. A. Shah, T. A. Lipo and B. -I. Kwon, "Modeling of Novel Permanent Magnet Pole Shape SPM Motor for Reducing Torque Pulsation," in *IEEE Transactions on Magnetics*, vol. 48, no. 11, pp. 4626-4629, Nov. 2012, doi: 10.1109/TMAG.2012.2197188.

[5] K. Matsuse and D. Matsuhashi, "New technical trends on adjustable speed AC motor drives," in *Chinese Journal of Electrical Engineering*, vol. 3, no. 1, pp. 1-9, 2017.

[6] Q. A. S. Syed and I. Hahn, "Analysis of flux focusing double stator and single rotor axial flux permanent magnet motor," *2016 IEEE International Conference on Power Electronics, Drives and Energy Systems (PEDES)*, Trivandrum, India, 2016, pp. 1-5, doi: 10.1109/PEDES.2016.7914324.

[7] Q. A. S. Syed and I. Hahn, "Influence of the Magnetic Bridges on the Flux Focusing Type Axial Flux Permanent Magnet Motor," *2018 IEEE Electrical Power and Energy Conference (EPEC)*, Toronto, ON, Canada, 2018, pp. 1-6, doi: 10.1109/EPEC.2018.8598318.

[8] Q. A. S. Syed, M. A. Shah, M. Ali, A. Ali, M. A. Shar, " Electromagnetic Analysis of the Skewed IPM Motor Using Multi-Sliced 2D Finite Element Method", *Pakistan Journal of Scientific Research*, vol. *5, no.* 2, pp. 113-118. https://doi.org/10.57041/d36n2h02

[9] H. -C. Liu, H. W. Kim, H. K. Jang, I. -S. Jang and J. Lee, "Ferrite PM Optimization of SPM BLDC Motor for Oil-Pump Applications According to Magnetization Direction," *IEEE Transactions on Applied Superconductivity*, vol. 30, no. 4, pp. 1-5, June 2020.

[10] Q. A. S. Syed, M. A. Solangi, and M. A. Shah, "Cogging torque reduction in induction motor through rotor skewing", Sir Syed University Research Journal of Engineering & Technology, vol. 15, no. 2, 2025. https://doi.org/10.33317/ssurj.709

[11] Abid, Muhammad Haseeb, Wasif Shafiq, Muhammad Dayem, and Hassan Riaz Khan. "Step-by-Step Installation of Solar Energy and Its Maintenance." *International Journal of Emerging Engineering and Technology* 4, no. 1 (2025): 1-5.

[12] Islam, Abdullah, Ahmad Saeed, Adeel Hassan, and Zeeshan Shahid. "AI-Powered Home Automation: A Simple and Smart Living Solution." *International Journal of Emerging Engineering and Technology* 4, no. 1 (2025): 6-10.

[13] Khan, M., Hasnain, S. K., & Jamil, M. "Digital Signal Processing: A Breadth-first Approach." River Publishers, 2022.

[14] Naseer, F., Khan, M. N., Tahir, M., Addas, A., & Aejaz, S. H. "Integrating deep learning techniques for personalized learning pathways in higher education."Heliyon,10(11), 2024.

[15] Naseer, F., Khan, M. N., Addas, A., Awais, Q., & Ayub, N. (2025). Game Mechanics and Artificial Intelligence Personalization: A Framework for Adaptive Learning Systems.Education Sciences,15(3), 2025

[16] Q. A. S. Syed, Spoke Type Axial Flux Permanent Magnet Motor and its Flux Switching Variants, Ph.D. dissertation, Friedrich-Alexander-Universität Erlangen-Nürnberg, Technische Fakultät, 2025. DOI: 10.25593/open-fau-2172.

[17] Q. A. S. Syed and M. A. Shah, "Starting Characteristic Analysis of the V-Shaped Interior Permanent Magnet Motor", Pakistan Journal of Engineering and Technology (PakJET), vol. 8, no. 4, pp. 1–5, Jan. 2026. https://doi.org/10.51846/vol8iss4pp1-5

[18] K. Matsuse and D. Matsuhashi, "New technical trends on adjustable speed AC motor drives," in *Chinese Journal of Electrical Engineering*, vol. 3, no. 1, pp. 1-9, 2017.

[19] Altair Engineering, Inc. Altair Flux 2D: Finite element software for low-frequency electromagnetic and thermal simulations, 2025. [Available]: https://altair.com/flux